IMTC 2005 - Instrumentation and Measurement
Technology Conference
Sorrento, Italy 24-27 April 2006

A Demodulation Technique for the Sensing Circuit of a MEMS Gyroscope

E. Nunzi[1], R. Antonello[2], P. Carbone[1], R. Oboe[3],
E. Lasalandra[4], G. Spinola[4], L. Prandi[4] and A. Rizzo[4]

[1]Department of Electronic and Information Engineering, University of Perugia,
[2]Department of Information Engineering, University of Padova,
[3]Dept. of Mechanical and Structural Engineering, University of Trento,
[4]STMicroelectronics S.r.l., MEMS Business Unit, 20010 Cornaredo (MI) - Italy

Abstract *– This paper deals with the design of a digital sensing interface for a MEMS gyroscope. In such devices, the information regarding the angular rate $\Omega_Z(t)$ experienced by the sensor is contained in a suppressed carrier– dual side band (SC–DSB) signal, which has $\Omega_Z(t)$ as modulating component. Hence, a demodulation must be carried out in order to retrieve a measurement of the angular rate. The demodulation process presented in the paper consists of a quantization stage of the SC–DSB signal, which is performed with a three–level band–pass $\Delta\Sigma$ converter, followed by a digital demodulation of the $\Delta\Sigma$ bit–stream with a given digital sequence. Several simulation results are reported to evaluate system performances.*

Keywords *– MEMS gyroscope, band–pass $\Delta\Sigma$ converters, demodulation logic*

I. INTRODUCTION

Micromachined gyroscopes are devices used to measure the angular velocity of rotating bodies. Almost all MEMS gyroscopes use vibrating elements to sense rotation: for this reason they are referred to *vibratory gyroscopes*. Regardless actual implementation, all vibratory gyroscopes obey to the same working principle, which can be analyzed with the aid of the model depicted in Fig.1 in the case of a gyroscope sensitive to rotation along a single axis. A *proof mass* is attached to a supporting structure through elastic suspensions that are compliant along two orthogonal axes (X',Y' axes) and rigid along the remaining directions: as a whole, the motion of the proof mass is constrained on a plane (X', Y' plane). This motion can be described by the coordinates $x(t)$, $y(t)$ defined on a frame fixed with the rotating structure ($Ox'y'z'$ in Fig. 1). A vibrating motion is induced along the axis X' (*drive axis*) by means of dedicated actuators. When the supporting structure rotates, the *Coriolis* force, $F_c(t)$, induces a motion along the orthogonal axis Y' (*sense axis*). The corresponding acceleration, $a_c(t)$, is proportional to the angular rate, $\Omega_Z(t)$, and to the drive axis velocity, $\dot{x}(t) \triangleq dx/dt$, i.e.:

$$a_c(t) = -2\Omega_z(t)\dot{x}(t). \quad (1)$$

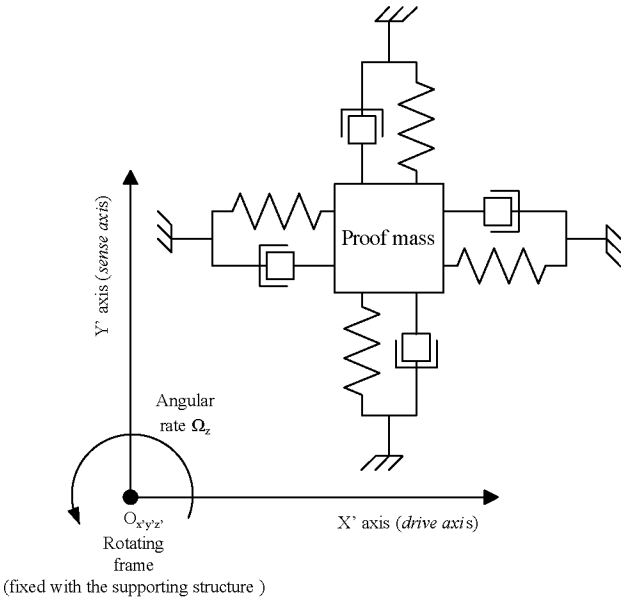

Fig. 1. Mass-spring-damper model of a vibrating gyroscope.

If $\dot{x}(t)$ is a sinusoid of frequency f_x and $\Omega_Z(t)$ is a low–pass signal of bandwidth BW lower than f_x, then $a_c(t)$ is a suppressed carrier–dual side band (SC–DSB) modulated signal, with $\dot{x}(t)$ as the carrier. In this case, the angular velocity $\Omega_z(t)$ can be retrieved by measuring $a_c(t)$ in the rotating frame and by demodulating it with a sinusoidal carrier that is locked in phase with $\dot{x}(t)$ (synchronous demodulation). The usual way to sense $a_c(t)$ is based on a closed loop control of the motion along the sense axis. With this method, the motion induced by the Coriolis force is nullified by a control force that is considered as an estimate of the Coriolis force and it is used to retrieve the angular rate. The closed loop control system can be implemented either in the analog or digital domains. Digital processing is usually preferred because of its reduced sensitivity to analog noise. In [1] the authors used a band–pass $\Delta\Sigma$ converter to digitize the control force. The designed $\Delta\Sigma$ converter has been proved to supply an adequate signal–to–noise

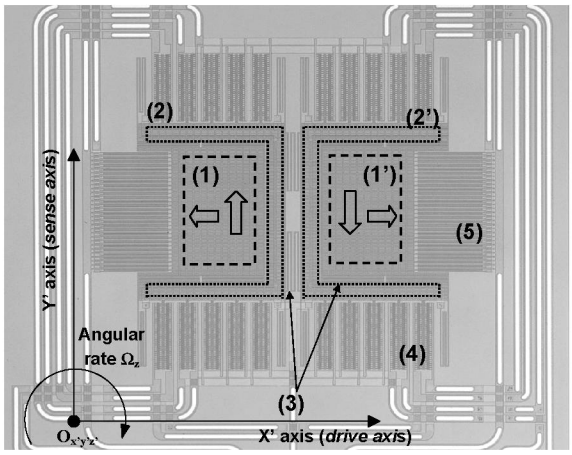

Fig. 2. Die photo of the STM gyroscope. (2),(2') are the U-shaped frames carrying the proof masses (1),(1'); (3) are folded beams suspensions; (4),(5) are electrodes for actuation/sensing.

(SNR) in the high frequency bandwidth. A closed loop sensing device has usually larger bandwidth, it achieves better linearity and it is more robust against temperature variations with respect to an open loop one. However, the synchronous demodulation condition requires a rigorous phase compensation of the phase delay introduced by the $\Delta\Sigma$ converter, which is a rather complex issue [2]. Thus, an open loop device is considered in this paper.

In particular, the mechanical sensing sensor output is quantized on a three–level band–pass $\Delta\Sigma$ converter. Since the $\Delta\Sigma$ in–band quantization noise power is lower than the in–band power of the noise affecting the sensor output signal, performance of the designed block is not affected by the quantization process. Moreover, the demodulation block is simplified since quantization is performed on three levels only.

II. STM MEMS GYROSCOPE

ST Microelectronics has developed a single axis surface-micromachined gyroscope with two proof masses and a symmetric structure, as shown in Fig.2. Each proof mass is made of a polysilicon plate attached to an U-shaped frame by means of elastic beams. Both elements are suspended above the silicon substrate. The frame can move along one axis (X'-axis/drive axis in Fig.2), dragging the attached proof mass in the same direction. Thanks to the spring suspensions, the proof mass can also move along an axis orthogonal to the previous one (Y'-axis/sense axis in Fig.2). To prevent air damping during the motion, the structure operates in a vacuum sealed package. Air gap capacitors with moving plates [3] are used both as actuators and sensors: in particular, comb fingers electrodes are employed along the drive axis, while parallel plates electrodes are used along the sense axis. Tab.I briefly summarizes the mechanical characteristics of the device.

A closed loop control system (whose details are provided in [4]) sustains an harmonic motion along the drive axis and controls the amplitude of $\dot{x}(t)$, so that $a_c(t) = -2\Omega_z(t)\dot{x}(t)$ is a SC–DSB signal and the scale factor of the sensor is kept constant.

TABLE I
MECHANICAL PARAMETERS OF THE STM MEMS GYROSCOPE

Drive part	
Mass (m_x)	$27.5 \cdot 10^{-9}\ kg$
Natural frequency ($\omega_x = 2\pi f_x$)	$2\pi \cdot 4100\ rad/s$
Quality factor (Q_x)	1250
Sense part	
Mass (m_y)	$7.8 \cdot 10^{-9}\ kg$
Natural frequency ($\omega_y = 2\pi f_y$)	$2\pi \cdot 4200\ rad/s$
Quality factor (Q_y)	650

The motion $y(t)$ along the sense axis of the proof mass, induced by an acceleration $a_y(t)$, is described by the following differential equation (second order resonant system):

$$\ddot{y}(t) + \frac{\omega_y}{Q_y}\,\dot{y}(t) + \omega_y^2\, y(t) = a_y(t), \tag{2}$$

or, equivalently, by the system frequency response:

$$H(\omega) = \frac{1}{(\omega_y^2 - \omega^2) + j\frac{\omega\,\omega_y}{Q_y}}, \tag{3}$$

where ω_y is the natural frequency and Q_y is the quality factor along the sense axis. The forcing term $a_y(t)$ is the sum of several contributions:

$$a_y(t) = \frac{1}{m_y}\left(F_c(t) + F_q(t) + F_b(t)\right), \tag{4}$$

where m_y is the proof mass, while the forcing terms are the *Coriolis force* F_c, the *quadrature error* F_q due to fabrication imperfections [3] and the force F_b due to *brownian noise* [5], [6]. In particular, it can be assumed that:

$$F_c(t) = -2m_y\Omega_z(t)\dot{x}(t) \tag{5}$$
$$F_q(t) = -k_{yx}x(t), \tag{6}$$

where k_{yx} is the asymmetric spring constant and $F_b(t)$ can be modelled as white Gaussian noise with zero mean and variance equal to $\sigma_b^2 = 841\ \mathrm{nV}^2$.

Since the model is linear, the output $y(t)$ can be evaluated by applying the superposition principle as

$$y(t) = y_c(t) + y_q(t) + y_b(t), \tag{7}$$

where each term of the sum can be computed by evaluating effects of the corresponding forcing term. In particular, by considering

$$x(t) = -A_x\cos(\omega_x\, t + \phi_x), \tag{8}$$

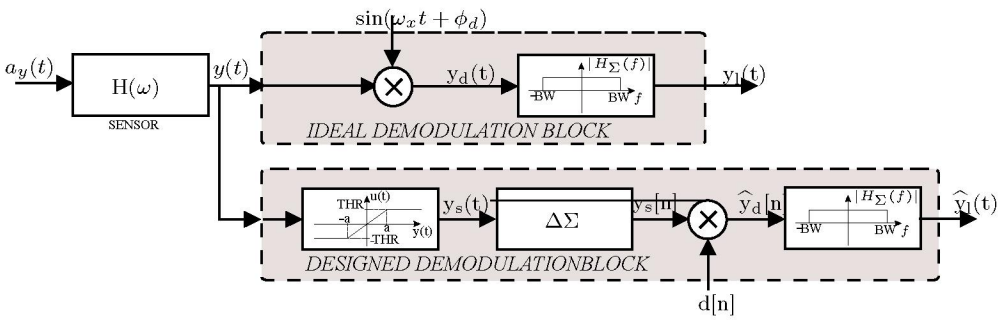

Fig. 3. Block diagram of the demodulation system designed for recovering $\Omega_z(t)$ from $y(t)$ (*DESIGNED DEMODULATION BLOCK*). The ideal demodulation process of a DSB signal (*IDEAL DEMODULATION BLOCK*) is reported for comparison purposes. In both schemes, the ideal filter with transfer function $H_\Sigma(\omega)$ passes only the components in the sensor frequency band.

and a sinusoidal angular rate

$$\Omega_z(t) \quad = \quad A_z \sin(\omega_z\, t + \phi_z), \tag{9}$$

the steady state value for $y_c(t)$ can be expressed as:

$$\begin{aligned} y_c(t) \quad &= \quad A_x\, A_z\, \omega_x\, |H(\omega_x + \omega_z)| \cdot \\ &\quad \cdot \cos\left[(\omega_x + \omega_z)t + \phi_x + \phi_z + \angle H(\omega_x + \omega_z)\right] + \\ &- \quad A_x\, A_z\, \omega_x\, |H(\omega_x - \omega_z)| \cdot \\ &\quad \cdot \cos\left[(\omega_x - \omega_z)t + \phi_x - \phi_z + \angle H(\omega_x - \omega_z)\right] \end{aligned} \tag{10}$$

Similarly, the steady state value for $y_q(t)$ becomes:

$$y_q(t) = |H(\omega_x)| A_{quad} \cos\left(\omega_x\, t + \phi_x + \angle H(\omega_x)\right) \tag{11}$$

where $A_{quad} \stackrel{\triangle}{=} A_x k_{yx}/m_y$. The displacement $y_b(t)$ induced by $F_b(t)$ is a white Gaussian noise colored by the filter with frequency response $H(j\omega)$: hence, $y_b(t)$ is a Gaussian noise with power spectral density (PSD) equal to $P_{y_b}(\omega) = \sigma_b^2 |H(\omega)|^2$.

The designed digital demodulation system processes the voltage signal $y(t)$ at the mechanical sensor output in order to recover the angular rate signal $\Omega_z(t)$.

III. DEMODULATOR DESIGN

Fig.3 shows the block diagram of the demodulator that has been designed to get $\Omega_z(t)$ from $y(t)$ (*DESIGNED DEMODULATION BLOCK*). For comparison purposes, the ideal demodulation process (*IDEAL DEMODULATION BLOCK*) of a SC–DSB signal is reported in the same figure. In both schemes, the ideal low–pass filter with frequency response $H_\Sigma(\omega)$ passes only the components in the sensor frequency band.

The useful base–band signal can be recovered by demodulating $y(t)$ with the sinusoidal carrier $\sin(\omega_x t + \phi_d)$, as indicated in Fig.3, inside the *IDEAL DEMODULATION BLOCK*. Since the demodulation and the filtering operations are linear processing systems, the in–band demodulated output $y_l(t)$ can be written as the sum of each in–band demodulated additive component of $y(t)$, i.e.

$$y_l(t) \quad = \quad y_{l_c}(t) + y_{l_q}(t) + y_{l_b}(t). \tag{12}$$

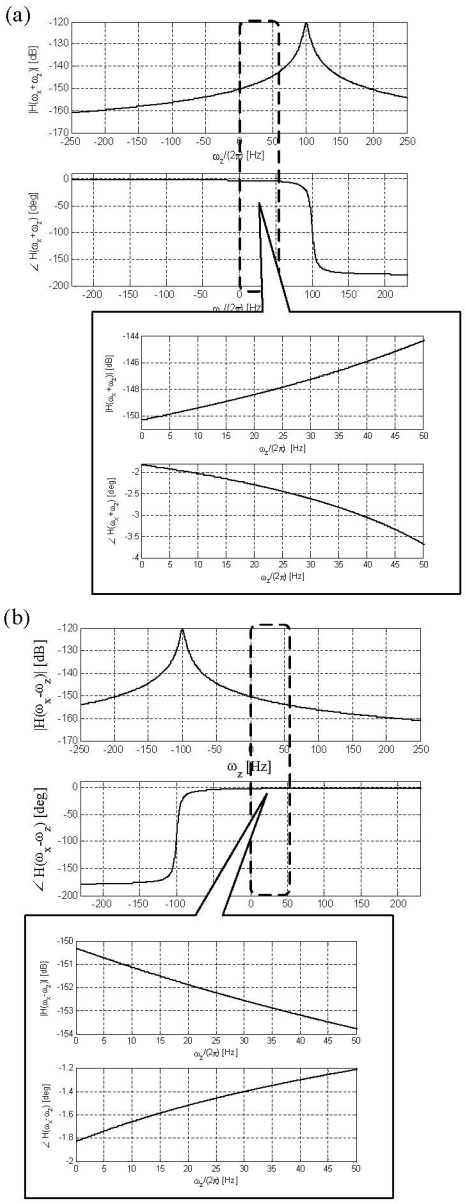

Fig. 4. Magnitude and phase of $H(\omega_x + \omega_z)$ (a) and $H(\omega_x - \omega_z)$ (b) with ω_z varying between 0 and $2\pi BW$.

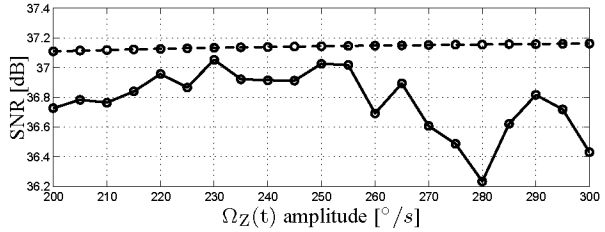

Fig. 5. SNR versus angular rate amplitude calculated at the modulator output by means of the *IDEAL* (dashed line) and *DESIGNED* (solid line) *DEMODULATION BLOCKS*. Simulations have been performed by assuming a sinusoidal angular rate with varying amplitude and frequency equal to 35 Hz, which is affected by an additive quadrature error with amplitude equal to $3FS$.

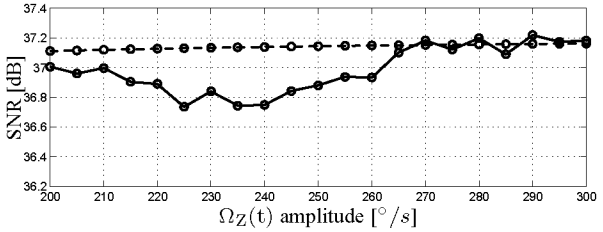

Fig. 6. SNR versus angular rate amplitude calculated at the modulator output by means of the *IDEAL* (dashed line) and *DESIGNED* (solid line) *DEMODULATION BLOCKS*. Simulations have been performed by assuming a sinusoidal angular rate with varying amplitude and frequency equal to 35 Hz not affected by any additive quadrature error.

In particular, by using (10) and (11), it is easy to verify that the in–band demodulated components due to the *Coriolis acceleration* and the quadrature component can be written, respectively, as:

$$\begin{aligned} y_{l_c}(t) &= -1/2\, A_x\, A_z\, \omega_x\, |H(\omega_x+\omega_z)| \cdot \\ &\cdot \sin(\omega_z\, t + \phi_x + \phi_z - \phi_d + \angle H(\omega_x+\omega_z)) + \\ &-1/2\, A_x\, A_z\, \omega_x\, |H(\omega_x-\omega_z)| \cdot \\ &\cdot \sin(\omega_z\, t - \phi_x + \phi_z + \phi_d - \angle H(\omega_x-\omega_z)) \end{aligned} \quad (13)$$

and

$$\begin{aligned} y_{l_q}(t) &= -1/2\, A_{quad}\, |H(\omega_x)| \cdot \\ &\cdot \sin(\phi_x + \angle H(\omega_x) - \phi_d). \end{aligned} \quad (14)$$

Fig. 4 (a) and (b) show that the attenuation and the delay introduced by $H(\omega)$ in the sensor frequency band are constant; in particular, the introduced delay is almost negligible.

It should be noticed that the quadrature error component affects $y_l(t)$ only with respect to the DC component. In particular, (14) shows that the quadrature error is negligible when a synchronous demodulation (i.e. $\phi_d = \phi_x$) is performed on the output signal $y(t)$. In fact, in this case the quadrature error amplitude depends only on $\sin(\angle\, H(\omega_x))$; since ω_x is far from the resonant frequency ω_y and the quality factor Q_y is sufficiently high (see Tab.I), it follows that $\angle H(\omega_x) \simeq 0$ and therefore $\sin(\angle\, H(\omega_x)) \simeq 0$: hence, the quadrature error is negligible. With regard to the Gaussian noise $y_{l_b}(t)$, it has been verified that this contribution is negligible when compared to $y_{l_c}(t)$ and $y_{l_q}(t)$.

The design of the demodulation circuitry has been realized in the discrete domain. In particular, since the useful modulated component of $y(t)$ has a bandwidth BW=100 Hz around the carrier frequency f_x=4100 Hz, a band–pass $\Delta\Sigma$ converter with center frequency equal to $f_0 = 0.25 f_x$ has been employed [1]. This value simplifies the digital demodulation stage since it implies a sampling frequency that is four times the f_x value. The $\Delta\Sigma$ topology allows the conversion of the input signal by introducing a low in–band quantization noise power. In particular, a three–level $\Delta\Sigma$ converter has been designed in order to simplify the demodulation logic circuitry, that involves signals which can assume only three logic values, i.e. -1, 0 or +1.

The *DESIGNED DEMODULATION BLOCK* in Fig.3 shows the designed demodulation circuitry that processes $y(t)$ by following the procedure described before for estimating $\Omega_Z(t)$. It should be noticed that the sensor output is amplified by a voltage gain stage which introduces an amplification gain K_{in} and saturates at $\pm THR = 1.5$V, the maximum nominal voltage value that amplifiers can tolerate. The amplification gain value has been set for guaranteeing the dynamic range (DR) of the useful–signal component to be within the DR of the voltage amplifier. This stage has a twofold purpose. The first is the maximization of the SNR at the $\Delta\Sigma$ output. In fact, the gain stage increases the useful–signal power in order to reduce the contribution of the in–band quantization noise power. The second is the reduction of the DR of $y_q(t)$ when it presents an amplitude larger than the useful–signal. The quadrature error component represents an undesirable signal at frequency f_x. The distortion phenomenon to which this signal component is subjected when its amplitude is larger than the DR of the voltage amplifier generates high frequency components that do not affect the in–band system performances.

Performances of the designed demodulation block have been evaluated in terms of signal–to–noise ratio (SNR) calculated at the demodulator output (SNR_{OUT}). The SNR of the useful base–band signal obtained by using the ideal and synchronous demodulation block has been evaluated for comparison purposes and is indicated as SNR_{IN}. Simulation results are shown in Figs.5–6, where solid lines represent SNR_{OUT}, while dashed–lines represent SNR_{IN}. These data have been obtained by applying a sinusoidal angular rate of frequency equal to 35 Hz to the sensor input and by calculating the SNR on $\hat{y}_l[n]$ and on $y_l(nT_s)$ using a frequency–domain approach. In particular, Figs.5 and 6 have been obtained by including and excluding, respectively, the additive quadrature error with $A_{quad} = 3FS$, by setting ϕ_x=0 rad and by varying the amplitude of $\Omega_Z(t)$ from 200°/s to 300°/s.

IV. CONCLUSIONS

In this paper the design of a digital demodulator for a MEMS gyroscope has been described. The demodulation process has been realized in the digital domain by quantizing the sensing–sensor output on a three–level band–pass $\Delta\Sigma$ converter and by sampling at a frequency value equal to four times the carrier signal. The converter input is pre–amplified by a saturating voltage gain stage that presents a dynamic range equal to that of the useful signal. The signal processing performed on the sensor output has been analyzed and the expression for the in-band signal component at the demodulator output has been explicitly given.

Presented simulation results confirm the validity of the proposed analysis and show that the proposed structure does not affect signal performance in terms of SNR since the power of the in–band quantization noise is lower than the power of the noise affecting the processed signal.

REFERENCES

[1] R. Oboe, R. Antonello, P. Carbone, E. Nunzi, E. Lasalandra, L. Prandi, and G. Spinola. Design of a delta-sigma bandpass demodulator for a z-axis mems vibrational gyroscope. In *IEEE/ASME International Conference on Advanced Intelligent Mechatronics*, pages 238–242, Monterey, CA, July 2005.

[2] J.A.E.P. van Engelen and J. van de Plassche. *Bandpass Sigma Delta Modulators (Stability Analysis, Performance and Design Aspects)*. Kluwer Academic Publishers, Dordrecht, The Netherlands, 1999.

[3] S. Park. *Adaptive Control Strategies for MEMS Gyroscopes*. PhD thesis, Univ. of California, Berkeley.

[4] R. Oboe, R. Antonello, E. Lasalandra, G. Spinola, and L. Prandi. Control of a z-axis mems vibrational gyroscope. In *Proc. AMC 2004*, pages 153–158, Kawasaki, Japan, March 2004.

[5] R. P. Leland. Mechanical-thermal noise in vibrational gyroscopes. In *Proc. ACC*, pages 3256–3261, Arlington, VA, June 25-27 2001.

[6] S. Merlo V. Annovazzi-Lodi. Mechanical-thermal noise in micromachined gyros. *Microelectronics Journal*, (30):1227–1230, 1999.